Electronic Supplementary Material (ESI) for Environmental Science: Atmospheres.

Chemical Functionality at the Liquid Surface of Pure Unsaturated Fatty Acids

Aisling C. Stewart, Martin J. Paterson, Stuart J. Greaves

Institute of Chemical Sciences, Heriot-Watt University, Edinburgh EH14 4AS, United Kingdom

Supporting Information

Contents

S1 Comparison of Force Fields 3

S2 Tests to determine the required slab thickness 5

S3 Side on Views of Slabs 6

S4 Work Flow for the Production and Equilibration of the Slabs 7

S5 Comparison of Fatty Acids Used 8

S6 SASA Results at Different Probe Sizes 9

S7 Block Analysis 11

S8 Thresholding Parameter for the SASA Analysis 12

S9 Error Values for the SASA results 13

S10 Orientational Analysis of the Annealing and Equilibration Process 14

S11 X and Y Density Analyses 16

References 17

S1 Comparison of Force Fields

When carrying out molecular dynamics calculations a range of force fields are available to describe the bonded and non-bonded interactions within molecules. In order to carry out the most accurate simulations of a given species it is important to select a force field that is both capable of simulating all of the required interactions, and does this in the way that is closest to the real world situation. In order to test the suitability of force fields for simulating a species, test simulations are carried out and physical properties extracted from these and compared to experimentally measurable quantities.

No force field is exhaustive in its list of parameters, and several of the force fields commonly in use (OPLS,[1] and many of the commonly used AMBER[2] and CHARMM[3] force fields, for example) do not contain a description of the dihedral interactions in a region where there are two C=C bonds close together (for example they lack a description of the -C=C-C-C= dihedral interaction). As such these cannot be used in simulations of any of the fatty acids here except for oleic acid. After having ruled out these force fields, tests were carried out using several force fields that were able to describe all the interactions in the molecules of interest. Bulk samples were generated and equilibrated (see main text for details of these processes) and analysis carried out to extract the densities and viscosities (see Table S1). These extracted quantities were compared to literature experimental values and the force field that most closely represented these (the General AMBER Force Field, GAFF[4]) was selected. Analysis was carried out on NPT equilibration runs (velocity Verlet algorithm[5] and Martyna-Tuckerman-Tobias-Klein pressure coupling,[6] 1 fs time step). These runs had been simulated for 5 ns after the densities of the samples had reached their equilibrium values.

Density/g mL^{-1}							
	Experimental (Literature)	Calculated			% Difference		
		Gromos43a1	Gromos54a7	GAFF	Gromos43a1	Gromos54a7	GAFF
Oleic Acid (298 K)[7]	0.89	1.03±0.00	0.91±0.00	0.86±0.00	16	2.3	-3.4
Oleic Acid (333 K)[8]	0.87	1.07±0.00	0.89±0.00	0.87±0.00	24	2.3	0.0
Linoleic Acid (298 K)[9]	0.902	0.96±0.00	0.92±0.00	0.88±0.00	6.7	2.2	-2.2
Linolenic Acid (298 K)[10]	0.914	1.00±0.00	0.95±0.00	0.90±0.00	8.7	3.3	-2.2
Stearidonic Acid (288 K)	0.93	0.98±0.00	0.96±0.00	0.92±0.00	5.4	3.2	-1.1
Viscosity/Cp							
	Experimental (Literature)	Calculated			% Difference		
		Gromos43a1	Gromos54a7	GAFF	Gromos43a1	Gromos54a7	GAFF
Oleic Acid (293 K)[11]	34.828	40.783±0.096	22.174±0.144	43.527±0.262	17.098	-36.333	24.977
Oleic Acid (303 K)[11]	15.921	37.851±0.188	36.263±0.135	42.147±0.239	137.74	127.76	164.73
Oleic Acid (313 K)[11]	8.805	63.446±0.138	17.034±0.257	12.848±0.418	620.5	93.48	45.91
Linoleic Acid (313 K)[12]	11.464	294.886±1.034	29.079±0.248	12.668±0.276	2472.2	153.65	10.502
Linoleic Acid (333 K)[12]	8.781	64.352±0.188	14.179±0.137	24.309±0.345	632.8	61.47	176.8

Table S1 Comparison of selected physical properties of the species studied with those calculated based on MD simulations employing the Gromos43a1,[13] Gromos54a7[14] and GAFF[4] force fields. In the left-hand columns of the table the raw values are shown. The right-hand columns show the deviation, of the calculated values from the experimental ones ($\boldsymbol{\Delta}_{\mathbf{value}} = \frac{\textbf{Simulated Value}-\textbf{Experimental Value}}{\textbf{Experimental Value}}\mathbf{x100}$).These deviations are expressed as a percentage.

S2 Tests to determine the required slab thickness

When setting the optimal size of a molecular dynamics (MD) simulation box with periodic boundary conditions (PBC) it is important to ensure that no molecule can interact with itself across the PBC. Thus the absolute minimum dimension of the box should be the maximum length of the molecule (~2.1 nm for oleic acid) + twice the length of the long range intermolecular interactions in the force field used. Similar considerations apply for the depth of a liquid ‘slab’ with vacuum on either side. The simulation must be sized so that a molecule affected by one vacuum-liquid interface should not be able to interact with one affected by the opposite vacuum-liquid interface; there should be molecules in between the interfaces that experience essentially bulk conditions. Tests were carried out to determine the number of molecules required in order to simulate a slab with two interfaces that were distinct from the bulk. Differing numbers of molecules were added to boxes of a cross section (xy) of 6.5x6.5 nm and a depth (z) proportional to the number of molecules being added, with 300 molecules corresponding to a cubic box (see Figure S1). These then underwent energy minimization and equilibration as bulk samples before being converted into slabs by expanding the size of the periodic box by a factor of three (see Methods section of the main text, and Figure S2a). The resulting samples then underwent further equilibration for 5 ns under NVT conditions, before partial density analysis was carried out, showing the concentrations of different functional groups at different distances from the center of the slab (z = 0).

From the graphs in Figure S1 it can be seen that for slabs containing 600+ molecules there is a distinct functional group density profile at the edges of the slab (higher absolute values of z), with this returning smoothly to bulk values as z → 0. When ≤450 molecules are used this distinction is less sharp, with the slabs appearing to have a greater amount of internal structure. This may indicate that not enough molecules have been included in the simulation in order for the two interfaces to be independent of each other and the main bulk. 600 molecules was found to be the ideal number to use in order to ensure that the behavior at a true interface could be modelled correctly whilst ensuring that the computational costs of the simulations did not become unnecessarily high.

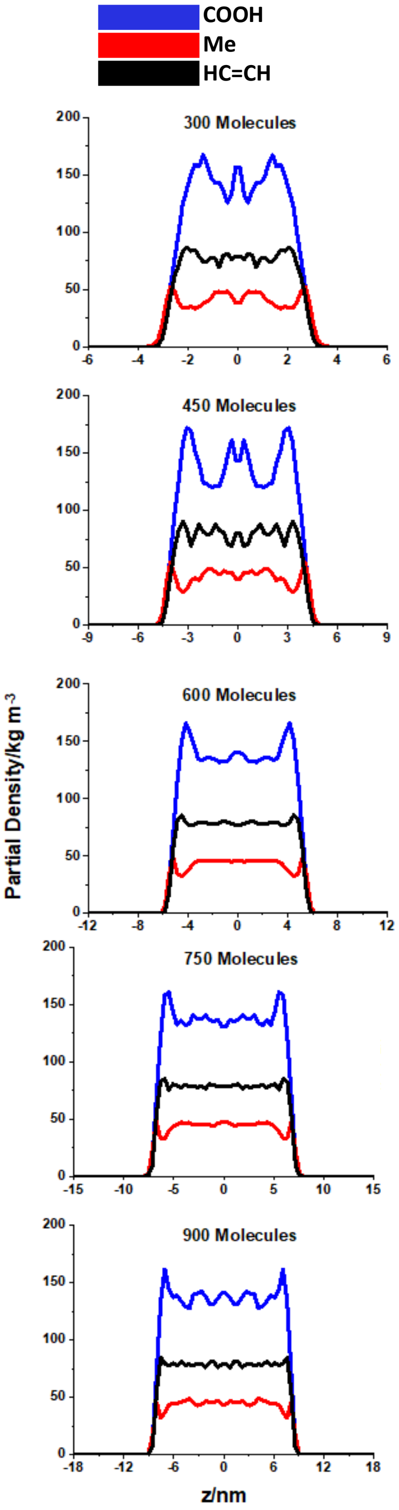

Figure S1 Partial density profiles for slabs with the same cross section but differing numbers of molecules and therefore different thicknesses. Analysis was carried out at the end of a 5 ns production run. The graphs shown have not been normalized, and the range of the x-axis (z coordinate in nm) is not the same on all plots. For further details see the main text.

S3 Side on Views of Slabs

A side-on view of a typical slab is shown in its PBC box in Figure S2a, the z axis of the simulation is vertical in the figure. As discussed in the main paper and Section S2 above the vacuum-liquid interfaces at the top and bottom of the slab are created by increasing the z coordinate of a bulk liquid simulation by a factor of three. Figure S2b shows side on views of slabs of each of the four fatty acids simulated.

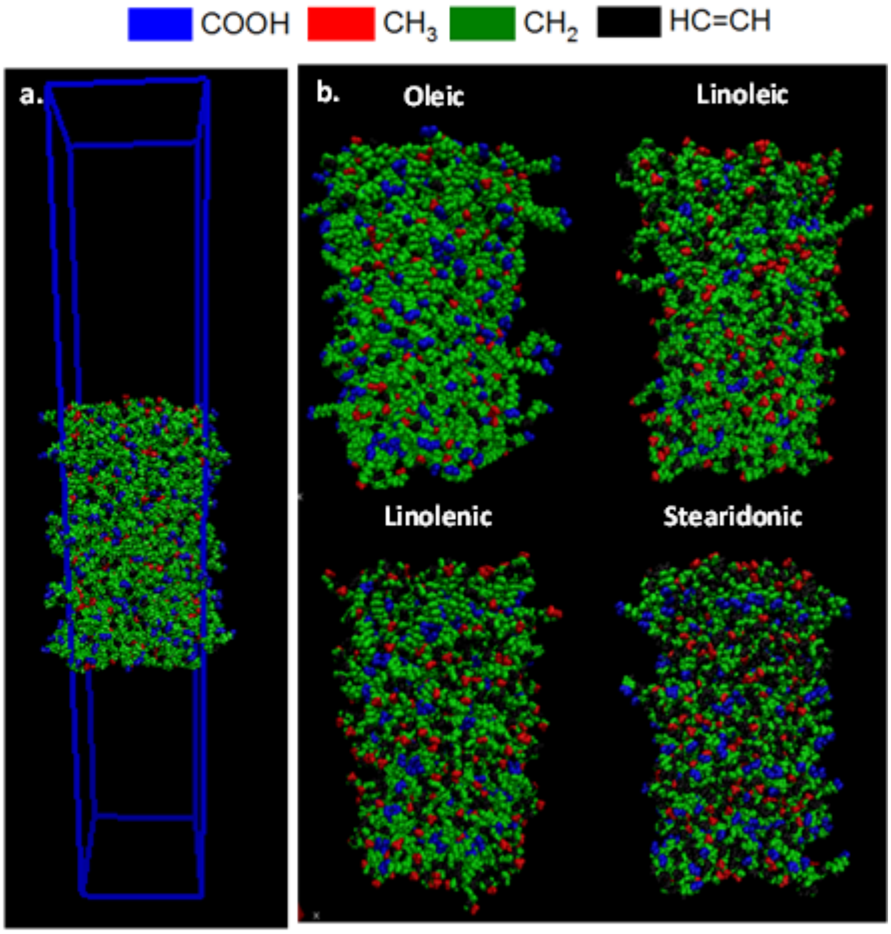

Figure S2 Side on views of fatty acid slabs with functional groups color coded in the same fashion as the main paper. **a**. An oleic acid slab at 298 K, showing the periodic box marked in blue. Areas of vacuum above and below the sample each have the same volume as the sample itself and form the interfaces with this that are discussed in the main text. **b.** Slabs of each of the acids at the end of 20 ns production runs at 298 K (top views are shown in Figure 2 of the main text). The increased number of methyl groups (red) and decreased number of carboxylic acid groups (blue) protruding from the top and bottom of these slabs can be seen and supports the idea of a non-statistical distribution of groups with respect to the surface.

S4 Work Flow for the Production and Equilibration of the Slabs

The aim of the work described in the main text is to investigate the positions of different groups with relation to the surfaces of fatty acid samples that have reached equilibrium, and therefore it was important to ensure that the samples on which the final analysis was carried out had reached equilibrium. As such a multi-step annealing process was carried out on the bulk samples before these were converted to slabs and subjected to a series of equilibration-annealing cycles, as described in the Methods section of the main text. Figure S3 shows pictorially the process for obtaining the production runs which are the main subject of this paper.

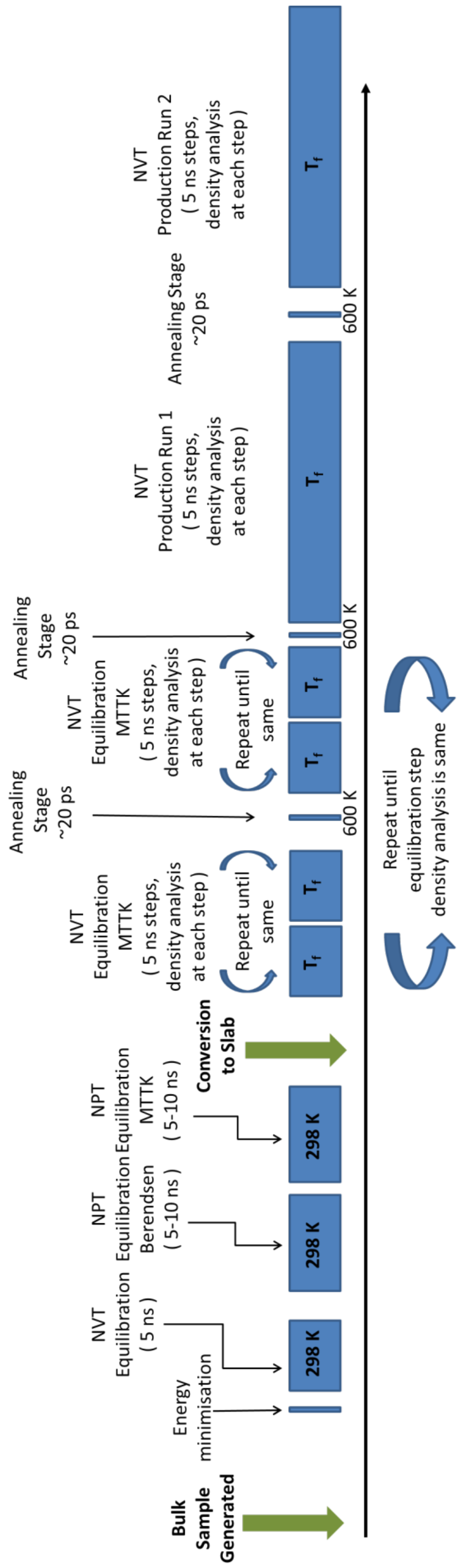

Figure S3 Schematic time line showing the order in which stages were carried out in the generation and equilibration of the samples. The first four stages involved energy minimization and equilibration of the bulk sample. Following this the periodic box was expanded to form interfaces with vacuum at the top and bottom of the liquid samples. Several rounds of NVT equilibration and annealing were carried out until the distributions of functional groups at the ends of consecutive stages were the same. Following this two 20 ns production runs were carried out, separated by an annealing stage.

S5 Comparison of Fatty Acids Used

The oleic acid family was chosen as oleic acid is one of the commonly studied components of aerosols; it is often used as a proxy for fatty acids in laboratory-based experiments. As the C=C moiety is highly reactive towards gas phase radical species this work set out to determine its surface activity compared with the other functional groups in a fatty acid molecule. Other unbranched C18 fatty acids were examined as these would differ only in the number of double bonds and have otherwise as similar structures as possible. All-*cis*-fatty acids were chosen, as the unsaturated fatty acids found in natural sources are commonly all *cis*- acids,[15] however, the presence of *cis*- C=C bonds makes molecules more bent and thus affects their properties. One of the most obvious differences in the properties of the different fatty acids studied is their melting and boiling points (Table S2). The temperatures used during the studies were chosen to study surface activity as a function of temperature, while ensuring that the acids were liquid during the time scale of the simulations.

Species	**Boiling Point/K (Pressure/mmHg)**	**Melting Point/K**
Oleic Acid	467-468 (1.2)[16]	286-287[16]
Linoleic Acid	503-505 (1)[9]	268[9]
Linolenic Acid	502-503 (16)[17]	262.6[18]
Stearidonic Acid	382 (760) – predicted[19]	216[20]

Table S2 Experimental melting and boiling points for the fatty acids studied

The diffusivities of the acids also vary as you increase the level of unsaturation, as the more bent molecules have different abilities to move past each other. However, the simulation protocol used ensures that there is sufficient time for all molecule types to be able to diffuse past each other in order to reach their equilibrium positions at the temperatures studied. This is demonstrated by the fact that for each of the slabs studied the two production runs were separated by an annealing step, with the partial densities of groups being the same for each of the production runs and different for the annealing step that separated them, indicating that the molecules must have been able to move past each other sufficiently in order to return to the distributions that they were in prior to annealing. Further evidence of the molecules having sufficient time to equilibrate can be shown by calculating the rotational autocorrelation functions for the samples.[21] These describe the correlation between the C1→C18 vectors in each of the molecules at time=0 with those at time=t and are shown in Figure S7. The exponential decay with time shows that the molecules are able to move freely.

The bent nature of the *cis*-fatty acids (especially linolenic and stearidonic acid) might be expected to allow for a case in which the two ends of the molecule could both be present at the surface. However, it was found that the majority of molecules that have an atom at the surface have only 1 or 2 atoms at the surface, and in the majority of those with 2 or more atoms at the surface the atoms are adjacent. There are only a few rare cases where both the COOH and the Me from the same molecule are at the surface. In the specific cases of linolenic & stearidonic acids, due to the very low number of COOH at the surface in these systems there are only one or two molecules per 20 ns trajectory where both end of the molecule are simultaneously present at the interface.

S6 SASA Results at Different Probe Sizes

SASA methods analyse the surface areas of different atom types that are accessible to a spherical probe of a given radius that makes contact with the interface from the vacuum side. The probe is inert and does not alter the surface it is probing, as such the SASA analysis cannot account for any changes to surface structure caused by the polarizing abilities of an incoming gas-phase species.

While the presence of a highly polarized radical could alter the equilibrium structure of a system, due to the short interaction time of a gas phase collider with the surface there is not sufficient time for the whole surface to rearrange, i.e. it would not change the configuration of the surface (revealed by the SASA analysis) to allow e.g. more COOH or C=C to be present. Any changes would be of a very small scale such as a small torsional motion in a Me to allow more favourable alignment of a C-H bond to the incoming radical. Any such rearrangement is also likely to be the prelude to reaction, aligning bonds to approach the required transition state structure. Due to the highly reactive nature of OH it would be unlikely to penetrate the surface any further than the SASA analysis, which uses a hard sphere.

The probe radius for the work shown in the main paper has been chosen to represent the size of an OH radical. OH is one of the most common reactive species in the atmosphere,[22] and is also commonly used in experimental surface scattering experiments,[23] thus allowing for the possibility of verifying the results presented experimentally. Varying the probe size can, however, potentially alter those atoms which are accessible at the surface to the probe and thus different reactive atmospheric species may find different groups to be available to them at the surface of an aerosol. Figure S4 shows the results of carrying out SASA analysis with a probe of size 0.20 nm, at 298 K. This represents the size of an ozone molecule approaching side-on, another species that commonly interacts with unsaturated groups of aerosols (ref).[24] This analysis was carried out on the same 20 ns production runs as for the probe = 0.15 nm work and using the same thresholding parameters (see Section S8 for details), with the results shown as an average across two 20 ns production runs, separated by an annealing step. It can be seen that the conclusions drawn for the 0.15 nm probe size are largely unchanged for the work using this larger probe: there is a relatively large methyl and very low COOH coverage for all acids and the HC=CH presence at the surface is very similar for both probe sizes. The main difference shown is for linoleic acid, which at the larger probe size has an even smaller COOH surface coverage than for probe radius = 0.15 nm, and an increased CH_2 coverage.

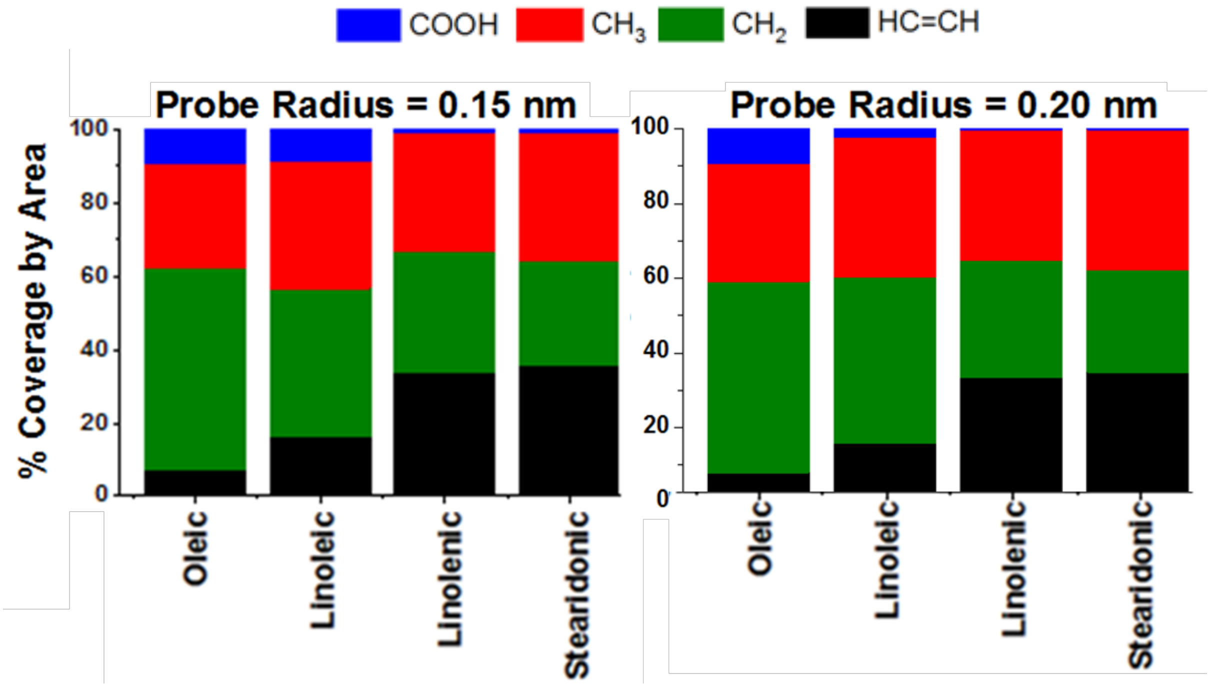

Figure S4 Comparison of SASA outputs for two different probe radii, at 298 K. For both sets of data, for each acid analysis has been carried out on the same two 20s production runs, and the results shown are an average of these. Thresholding has been carried out as described in Section S8.

S7 Block Analysis

Block covariance analysis[25] was used to determine the relaxation times of the liquids and to thus ensure that the sampling frequency of the SASA analysis was appropriate. SASA values were calculated for each of the runs for times < 2.5 ns, in order to allow equilibration of the sample at the temperature of interest.

The block analysis is carried out by dividing the production run into blocks of length variable length b, with the total number of blocks defining n_b. The mean of each of these blocks ($\bar{S}$) is calculated from the SASA results for the individual frames (S_i) within the block.

$$\bar{S}_b = \frac{1}{b}\sum_{i=0} S_i$$

The variance of each block is then calculated and then averaged according to

$$\sigma^2 (\overline{S_b}) = \frac{1}{n_b}\sum_{b=1}^{n_b}(\bar{S}_b - \bar{S}_T)^2$$

It can be seen from Figure S5 that for smaller step sizes there is a higher degree of correlation between data at neighbouring steps, with this correlation decreasing as step size increases. A sampling period of 100 ps was chosen when selecting the frames used in the SASA analysis presented in the main text, as this was large enough to avoid a high degree of correlation between data points, whilst still allowing for enough data points to allow for a good statistical analysis.

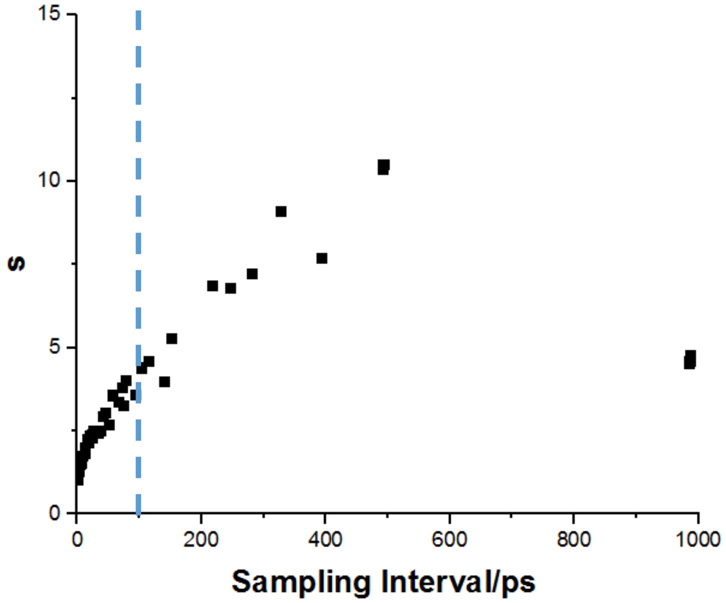

Figure S5 Block analysis applied to one of the linoleic production runs at 298 K. The chose sampling period is shown with a dashed blue line.

S8 Thresholding Parameter for the SASA Analysis

Within the bulk there will be pores that may be accessible to a probe of a small enough radius. Contact of the probe with atoms that are in these pores may lead to them being recorded as present at the surface when in reality this is not the case. To differentiate between atoms that are present at the interface and those that are in pores within the bulk sample a threshold is set for the minimum contact that must be had between the probe and an atom in order for this to be included in the surface count.

The threshold value needs to be selected to effectively separate the true interface from spurious signals in the bulk.[26] A value approaching zero will sample both the surface and the bulk pores, whereas a threshold value that is too large would lead to some of the atom-probe contacts being disregarded. Tests were carried out in order to find the ideal value for this threshold parameter, by changing its value and recording how the total number of atom hits counted varied. Analysis was run on both the slabs and on the bulk samples from which these were generated, with Figure S6 showing one example of these. A threshold value of 0.05 nm^2 was chosen based on these tests. At this value < 1% of the signal recorded comes from the bulk, however, the threshold is still low enough to ensure that large amounts of signal from the surface are not being disregarded.

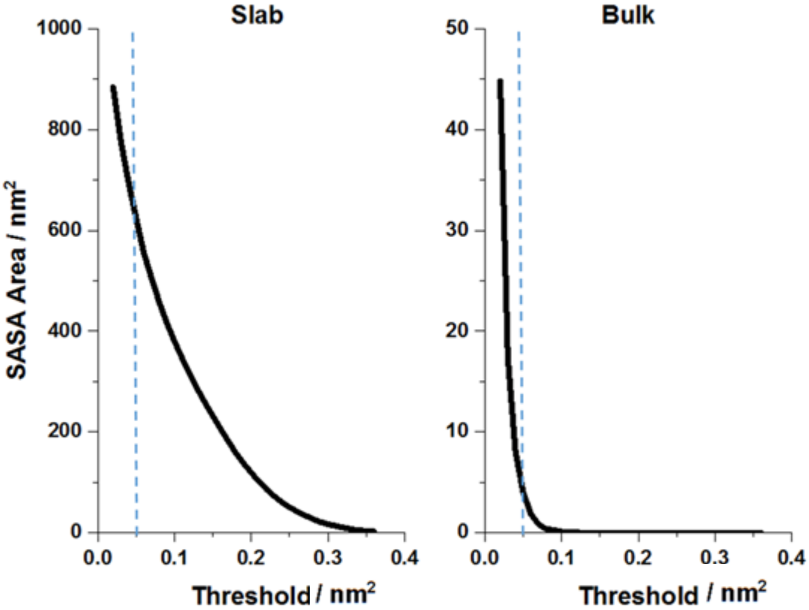

Figure S6 Plots of the threshold value versus total surface area recorded, for oleic acid at 298 K, for the slab (left) and the bulk sample before being converted into a slab (right). Note the difference in y-axis scale between the two graphs. The blue dashed lines represent the threshold value chosen for the analysis described in the main text. Similar plots could be drawn for the other acids, with this threshold value found to be valid for all the species discussed.

S9 Error Values for the SASA results

Table S3, Table S4, and Table S5 below show the absolute values (and errors) for the SASA analyses that were used to make Figure 3 of the main paper. These represent the results of carrying out SASA analysis on the 20 ns production runs and then averaging the results over two trajectories for each temperature and acid. The error values shown are standard errors over the two runs. Analysis was only carried out at times >2.5 ns to ensure the slabs were fully equilibrated prior to data extraction.

273 K	Oleic acid		Linoleic acid		Linolenic acid		Stearidonic acid	
	Mean	Error	Mean	Error	Mean	Error	Mean	Error
COOH	7.868	0.339	9.094	0.249	0.451	0.042	0.223	0.099
Me	30.941	0.145	34.372	0.243	34.343	0.506	36.955	0.091
HC=CH	7.521	0.170	15.567	0.189	32.879	0.275	34.603	0.112
CH_2	53.669	0.022	40.966	0.184	32.326	0.187	28.219	0.077

Table S3 Absolute values and errors for the SASA analysis of fatty acids at 273 K

298 K	Oleic acid		Linoleic acid		Linolenic acid		Stearidonic acid	
	Mean	Error	Mean	Error	Mean	Error	Mean	Error
COOH	9.147	0.039	8.441	0.366	0.467	0.014	0.3673	0.069
Me	28.185	0.1935	34.724	0.099	32.822	0.455	35.344	0.465
HC=CH	7.627	0.045	16.192	0.477	33.769	0.174	35.850	0.326
CH_2	55.039	0.188	40.640	0.209	32.940	0.295	28.438	0.069

Table S4 Absolute values and errors for the SASA analysis of fatty acids at 298 K

333 K	Oleic acid		Linoleic acid		Linolenic acid		Stearidonic acid	
	Mean	Error	Mean	Error	Mean	Error	Mean	Error
COOH	10.595	0.115	9.029	0.087	0.796	0.480	0.624	0.075
Me	26.084	0.195	31.560	0.111	31.166	1.885	32.729	0.430
HC=CH	7.412	0.094	16.611	0.280	33.339	0.782	37.267	0.126
CH_2	55.907	0.014	42.798	0.082	34.696	2.188	29.377	0.228

Table S5 Absolute values and errors for the SASA analysis of fatty acids at 333 K

S10 Orientational Analysis of the Annealing and Equilibration Process

In order to confirm that the preferential ordering of functional groups described in the main text is truly a function of the presence of the interfaces, it is necessary to assess the orientational preference for the molecules with relation to each other. Some molecules could become trapped in regions of higher order due to, for example, hydrogen bonding with each other, and thus become unable to reach their equilibrium positions. In Figure S7 we demonstrate that this is not the case for our systems, by analyzing the orientations of the molecules during the two production runs and the annealing step between them. In the figure we show this for one example system, stearidonic acid at 298 K, however, analogous work has been carried out on the other acids and temperatures, with near-identical results.

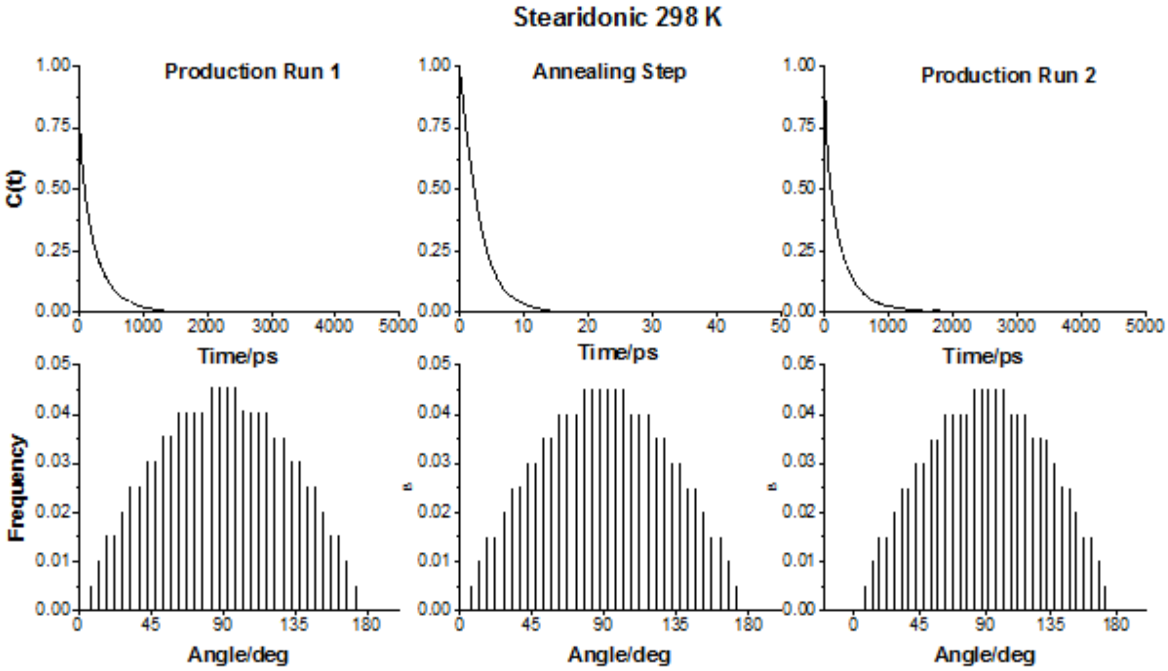

Figure S7 Top row: rotational ACFs for stearidonic acid for its two final production runs (total run time 20 ns) and the annealing step that separated them, see text for details. Bottom row: histograms of the distributions of angles between the molecular axis (COOH-Me / C1-C18 vector) and the z-axis for the same three trajectories.

The top row of Figure S7 shows the results of calculating the rotational autocorrelation function (ACF) for each of the runs (using gmx rotacf). This function describes how the direction in which a series of vectors points at time = t is related to the direction in which they were pointing at time t = 0. Here the vectors chosen to represent the 'molecular axis' i.e. the vector between the carbon of the methyl group and the carbonyl carbon (C1-C18) in each of the stearidonic acid molecules. The fact that each of the ACFs drops quickly (and in the case of the production runs, within the 2.5 ns that is not included in the main analysis of each of the runs) to zero demonstrates that the molecules are not trapped in a particular orientation. This happens ~100 times more rapidly in the annealing step, as would be expected due to the increased temperature, and again supports the conclusion that preferential ordering of molecules is destroyed during this step. The surface preference of the different functional groups reported here is thus decoupled from the orientation of the molecules in the simulation.

The bottom row of Figure S7 shows histograms of the distributions of angles between the molecular axes and the z-axis (normal to the interface, calculated using gmx gangle). The broad distribution of alignment angles also demonstrates that there is no preferential orientation of the molecular axis during the simulations, and so confirms the separation of molecular orientation and surface activity.

S11 X and Y Density Analyses

The partial density analysis in the main text focusses how the densities of different functional groups change on moving along the z direction, perpendicular to the interfaces. Similar analysis has been carried out along the y and x dimensions, parallel to the surface. Non-isotropic functional group distributions observed in these directions would indicate that the ordering discussed in the main text is not purely a result of the presence of the interface, but of fatty acid molecules having a favourable alignment with respect to each other. In this analysis, however, only isotropic functional group distributions were observed for all slabs in the x and y directions.

Figure S8 shows one example of this analysis, for the oleic acid slab at 298 K. Analysis has been carried out in a completely analogous way to that described for the z density analysis in the main text, using an average of the two 20 ns production runs and times within these > 2.5 ns. The results shown here have been positive/negative direction symmetrised, but otherwise left unnormalised for clarity. It should be noted that because of the periodic boundary conditions, there is no 'edge' of the slab in the x and y directions, and thus the functional group concentrations do not fall to zero at any value of x or y. The isotropic distributions in Figure S8 do not show any evidence of ordering in the x and y directions.

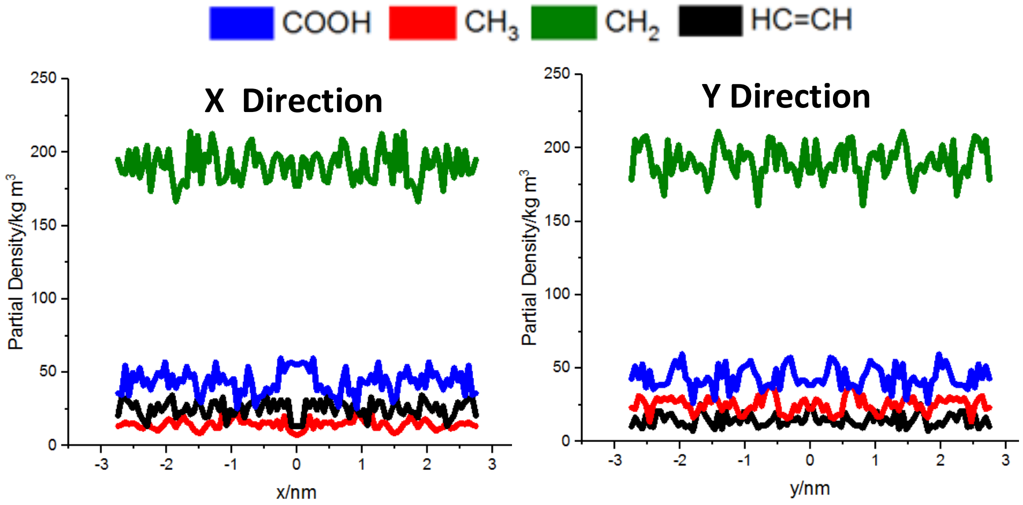

Figure S8 x and y density analyses for an oleic acid slab at 298 K.

References

(1) Beveridge, D. L.; Jorgensen, W. L. The OPLS (Optimized Potentials for Liquid Simulations) Potential Functions for Proteins, Energy Minimizations for Crystals of Cyclic Peptides and Crambin. *Annu. Rev. Biophys. Bioeng* **1988**, *110* (6), 39. https://doi.org/DOI: 10.1021/ja00214a001.

(2) Pearlman, D. A.; Case, D. A.; Caldwell, J. W.; Ross, W. S.; Cheatham, T. E. I.; DeBolt, S.; Ferguson, D.; Seibel, G.; Kollman, P. AMBER, a Package of Computer Programs for Applying Molecular Mechanics, Normal Mode Analysis, Molecular Dynamics and Free Energy Calculations to Simulate the Structural and Energetic Properties of Molecules. *Comp. Phys. Commun.* **1995**, *91*, 1–41. https://doi.org/https://doi.org/10.1016/0010-4655(95)00041-D.

(3) Brooks, B. R.; Bruccoleri, R. E.; Olafson, B. D.; States, D. J.; Swaminathan, S.; Karplus, M. CHARMM: A Program for Macromolecular Energy, Minimization, and Dynamics Calculations. *J. Comp. Chem.* **1983**, *4*, 187–217. https://doi.org/10.1002/jcc.540040211.

(4) Wang, J.; Wolf, R. M.; Caldwell, J. W.; Kollman, P. A.; Case, D. A. Development and Testing of a General Amber Force Field. *J. Comput. Chem.* **2004**, *25* (9), 1158–1174. https://doi.org/10.1002/jcc.20035.

(5) Swope, W. C.; Andersen, H. C.; Berens, P. H.; Wilson, K. R. A Computer-Simulation Method for the Calculation of Equilibrium-Constants for the Formation of Physical Clusters of Molecules: Application to Small Water Clusters. *J. Chem. Phys.* **1982**, *76* (1), 637–649. https://doi.org/https://doi.org/10.1063/1.442716.

(6) Martyna, G. J.; Tobias, D. J.; Klein, M. L. Constant Pressure Molecular Dynamics Algorithms. *J. Chem. Phys* **1994**, *101* (5), 4177–4189. https://doi.org/https://doi.org/10.1063/1.467468.

(7) Sagdeev, D.; Gabitov, I.; Isyanov, C.; Khairutdinov, V.; Farakhov, M.; Zaripov, Z.; Abdulagatov, I. Densities and Viscosities of Oleic Acid at Atmospheric Pressure. *JAOCS, J. Am. Oil Chem. Soc.* **2019**, *96* (6), 647–662. https://doi.org/10.1002/aocs.12217.

(8) Noureddini, H.; Teoh, B. C.; Clements, L. D. Densities of Vegetable Oils and Fatty Acids. *J. Am. Oil Chem. Soc.* **1992**, *69*, 1184–1188. https://doi.org/10.1007/BF02637677.

(9) Sigma Aldrich Product Catalogue: Linoleic Acid, Sigma Aldrich, Merck KGaA, St Louis, USA. https://www.sigmaaldrich.com/GB/en/product/sigma/l1376

(10) Sigma Aldrich Product Catalogue: Linolenic Acid, Sigma Aldrich, Merck KGaA, St Louis, USA. https://www.sigmaaldrich.com/GB/en/product/sigma/l2376.

(11) Sagdeev, D.; Gabitov, I.; Isyanov, C.; Khairutdinov, V.; Farakhov, M.; Zaripov, Z.; Abdulagatov, I. Densities and Viscosities of Oleic Acid at Atmospheric Pressure. *J. Am. Oil Chem. Soc.* **2019**, *96*, 647–662. https://doi.org/10.1002/aocs.12217.

(12) Rabelo, J.; Batista, E.; Meirelles, F. vi. W.; Cavaleri, A. J. A. Viscosity Prediction for Fatty Systems. *J. Am. Oil Chem. Soc.* **2000**, *77*, 1255–1262. https://doi.org/10.1007/s11746-000-0197-z.

(13) See-Wing Chiu, S.-W.; Pandit, S. A.; Scott, H. L.; Jakobsson, E. An Improved United Atom Force Field for Simulation of Mixed Lipid Bilayers. *J. Phys. Chem. B* **2009**, *113*, 2748–2763. https://doi.org/10.1021/jp807056c.

(14) Schmid, N.; Eichenberger, A. P.; Choutko, A.; Riniker, S.; Winger, M.; Mark, A. E.; Van Gunsteren, W. F. Definition and Testing of the GROMOS Force-Field Versions 54A7 and 54B7. *Eur. Biophys. J.* **2011**, *40* (7), 843–856. https://doi.org/10.1007/s00249-011-0700-9.

(15) Kenar, J. A.; Moser, B. R.; Lis, G. R. Naturally Occuring Fatty Acids. In *Fatty Acids: Chemistry, Synthesis, and Applications*; Ahmad, M. U., Ed.; Elsevier Inc.: Libertyville, 2017; pp 39–43.

(16) Sigma Aldrich Product Catalogue: Oleic Acid, Sigma Aldrich, Merck KGaA, St Louis, USA.

(17) Sigma Aldrich Product Catalogue:Linolenic Acid, Sigma Aldrich, Merck KGaA, St Louis, USA.

(18) Holman, R. T.; Elmer, O. C. The Rates Of Oxidation Of Unsaturated Fatty Acids And Esters. *J. Am. Oil Chem. Soc.* **1947**, *24*, 127–129. https://doi.org/10.1007/BF02643258.

(19) 6,9,12,15-Octadecatetraenoic Acid, BOC Chemicals, Shirley, USA.

(20) Guil-Guerrero, J. L. Stearidonic Acid (18_4n-3)_ Metabolism, Nutritional Importance, Medical Uses and Natural Sources. *Eur. J. Lipid Sci. Technol.* **2007**, *109*, 1226–1236. https://doi.org/10.1002/ejlt.200700207.

(21) Allen, M. P.; Tildesley, D. J. *Computer Simulations of Liquids*; Oxford Science Publications: Oxford, 1987.

(22) Li, M.; Karu, E.; Brenninkmeijer, C.; Fischer, H.; Lelieveld, J.; Williams, J. Tropospheric OH and Stratospheric OH and Cl Concentrations Determined from CH4, CH3Cl, and SF6 Measurements. *npj Clim. Atmos. Sci.* **2018**, *29*, 1–7. https://doi.org/10.1038/s41612-018-0041-9.

(23) Tesa-Serrate, M. A.; Smoll, E. J.; Minton, T. K.; McKendrick, K. G. Atomic and Molecular Collisions at Liquid Surfaces. *Annu. Rev. Phys. Chem.* **2016**, *67* (1), 515–540. https://doi.org/10.1146/annurev-physchem-040215-112355.

(24) Rogge, W. F.; Mazurek, M. A.; Hildemann, L. M.; Cass, G. R.; Simoneit, B. R. T. Quantification of Urban Organic Aerosols at a Molecular Level: Identification, Abundance and Seasonal Variation. *Atmos. Environ. Part A, Gen. Top.* **1993**, *27* (8), 1309–1330. https://doi.org/10.1016/0960-1686(93)90257-Y.

(25) Romo, T. D.; Grossfield, A. Block Covariance Overlap Method and Convergence in Molecular Dynamics Simulation. *J. Chem. Theory Comput.* **2011**, *7* (8), 2464–2472. https://doi.org/https://doi.org/10.1021/ct2002754.

(26) Tesa-Serrate, M. A.; Marshall, B. C.; Smoll, E. J.; Purcell, S. M.; Costen, M. L.; Slattery, J. M.; Minton, T. K.; McKendrick, K. G. Ionic Liquid-Vacuum Interfaces Probed by Reactive Atom Scattering: Influence of Alkyl Chain Length and Anion Volume. *J. Phys. Chem. C* **2015**, *119* (10), 5491–5505. https://doi.org/10.1021/jp5126238.